Supporting Information

Oxygen vacancies induced low overpotentials of Ag/CeO_2 for electrocatalytic evolution of oxygen and hydrogen

Ajit Kumar Dhanka[a], Mayank Tiwari[b], Prashant Kumar Bhartiya[c], Balaram Pani[d] Nityananda Agasti[a,*], Debabrata Mishra[#,*]

[a ,*] Department of Chemistry, University of Delhi, North Campus, Delhi 110007, India

[b,#] Department of Physics and Astrophysics, University of Delhi, Delhi 110007, India

[c] Delhi School of Climate Change and Sustainability, Institution of Eminence (IOE), University of Delhi, Delhi 110007, India

[d] Department of Chemistry, Bhashkaracharya College of Applied Sciences, University of Delhi, Dwarka, New Delhi, 110075, India.

SUPPORTING INFORMATION CONTENT

TABLE OF CONTENTS

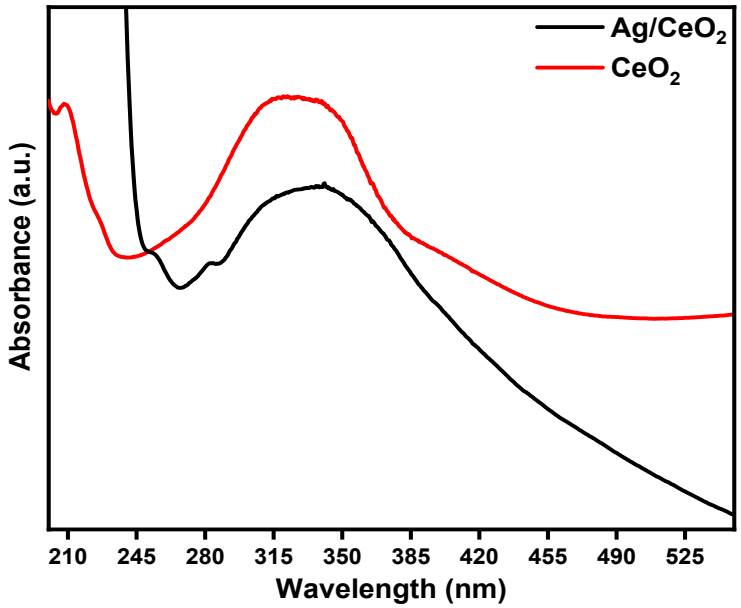

Fig. S1 UV-vis spectra of CeO_2 and Ag/CeO_2 nanocomposites.

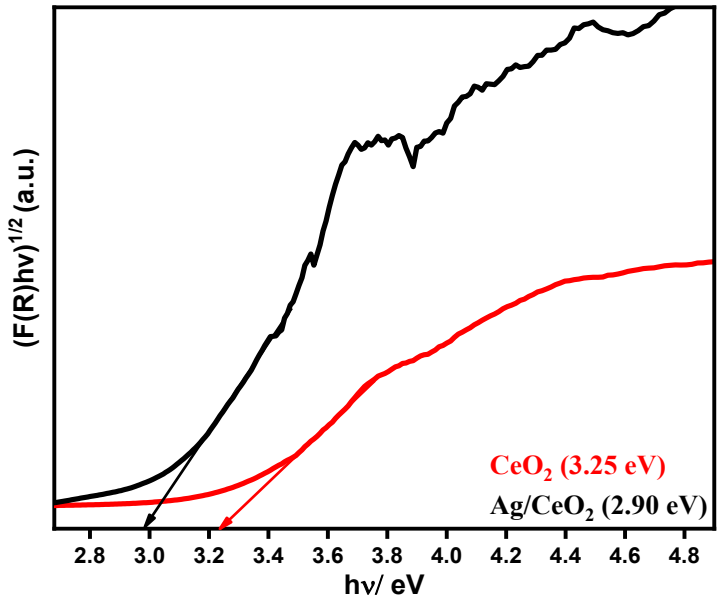

Fig. S2 Calculated band gap by UV-vis diffuse reflectance spectra (DRS) of CeO_2 and Ag/CeO_2 nanocomposites.

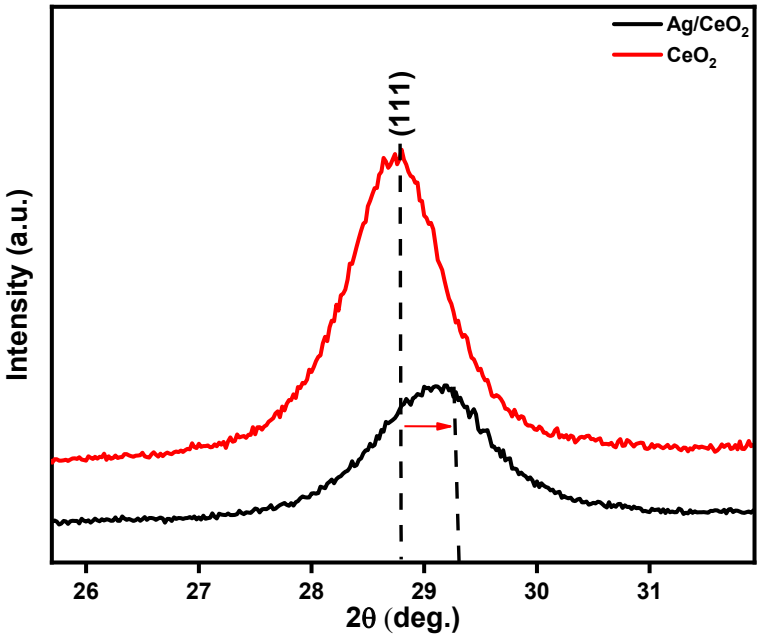

Fig. S3 Variation in intensity, broadening and shifting of PXRD peaks of CeO_2 and Ag/CeO_2.

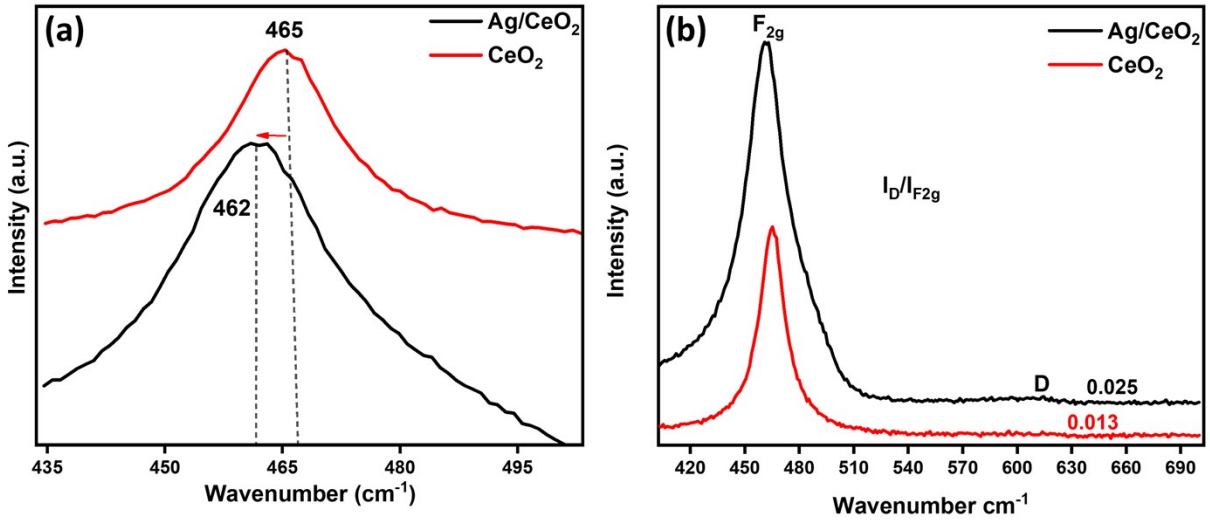

Fig. S4 Variation in intensity, broadening and shifting of Raman peaks of CeO_2 and Ag/CeO_2 and (b) calculated the integrated area of the D peak to the F_{2g} peak for CeO_2 and Ag/CeO_2 by I_D/I_{F2g} [1].

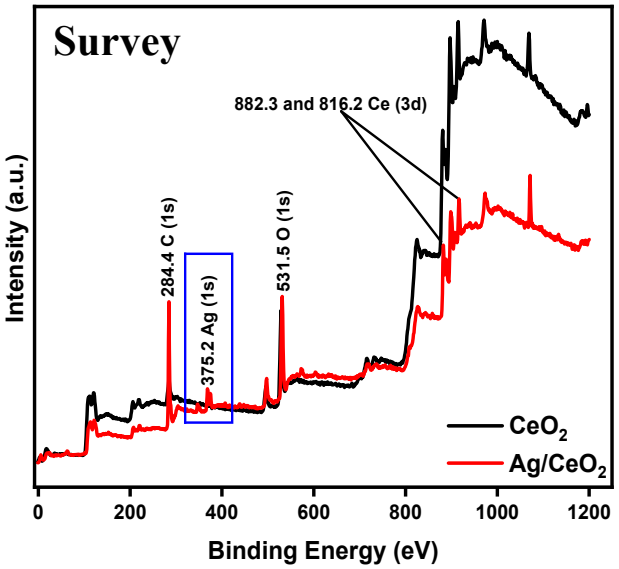

Fig. S5 The XPS survey of CeO_2 and Ag/CeO_2 nanocomposites.

The total cerium ions integral area of Ce 3d divide by the area of each peak[2,3]. It is calculated that 17.89% of Ce^{+3} for Ag/CeO_2 and is higher than 13.92% of the CeO_2. That means the addition of Ag causes the increase of oxygen vacancies in CeO_2.

$$[Ce^{+3}] = \frac{(Ce^{+3})Area}{\sum (Ce^{+4} + Ce^{+3})\ Area} \times 100$$

Table S1 High-resolution Ce 3d XPS results. The listed-out figures are the binding energies (BE) and the area of each peak. The ratio of Ce^{+3} / Ce^{+3} + Ce^{+4} was calculated to illustrate the content of oxygen vacancy around Ce^{+3} sites on the catalyst surface.

Peaks assignment	**Binding energy (eV)**	**Ag/CeO_2 (Area)**	**CeO_2 (Area)**
U	881-882	13048.3	14323.89
U’	884-885	7781.8	6593.19
U’’	887- 888	9114.15	10379.9
U’’’	897- 898	10917.54	10987.85
V	900-901	5720.20	7015.92
V’	902-903	4407.05	3264.08
V’’	905-906	11210.04	11593.14
V’’’	915-917	6531.96	6620.91
V’ and U’	**Total area of Ce^{3+}**	**12189.05**	**9857.27**
V’’’, V’’, V, U’’’, U’’, U	**Total area of Ce^{4+}**	**55941.99**	**60921.61**
	Total of Ce^{+3} + Ce^{+4}	**68131.04**	**70778.88**
% of Ce^{+3} from Ce 3d = Ce^{+3}/ Ce^{+3} + Ce^{+4}		**17.89**	**13.92**

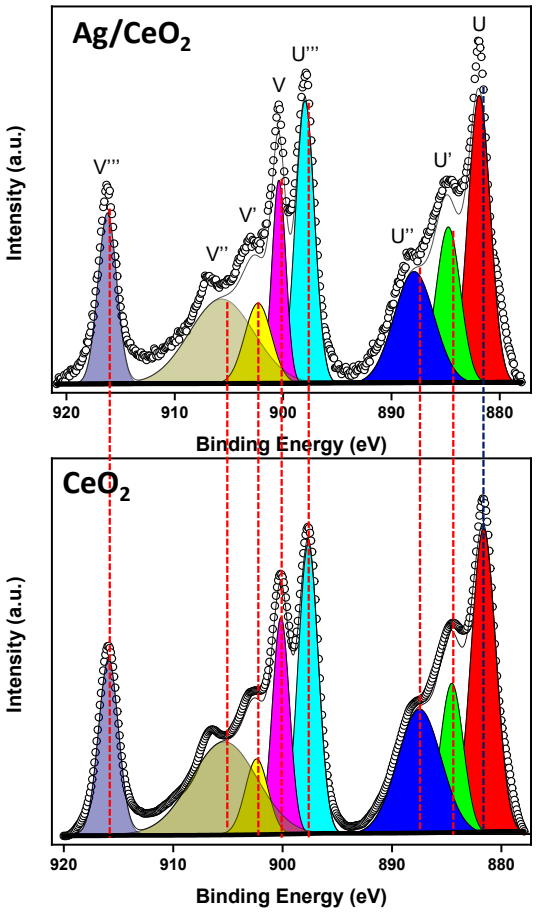

Fig. S6 High-resolution XPS spectra of Ce 3d comparative study for (a) Ag/CeO_2 and (b) CeO_2.

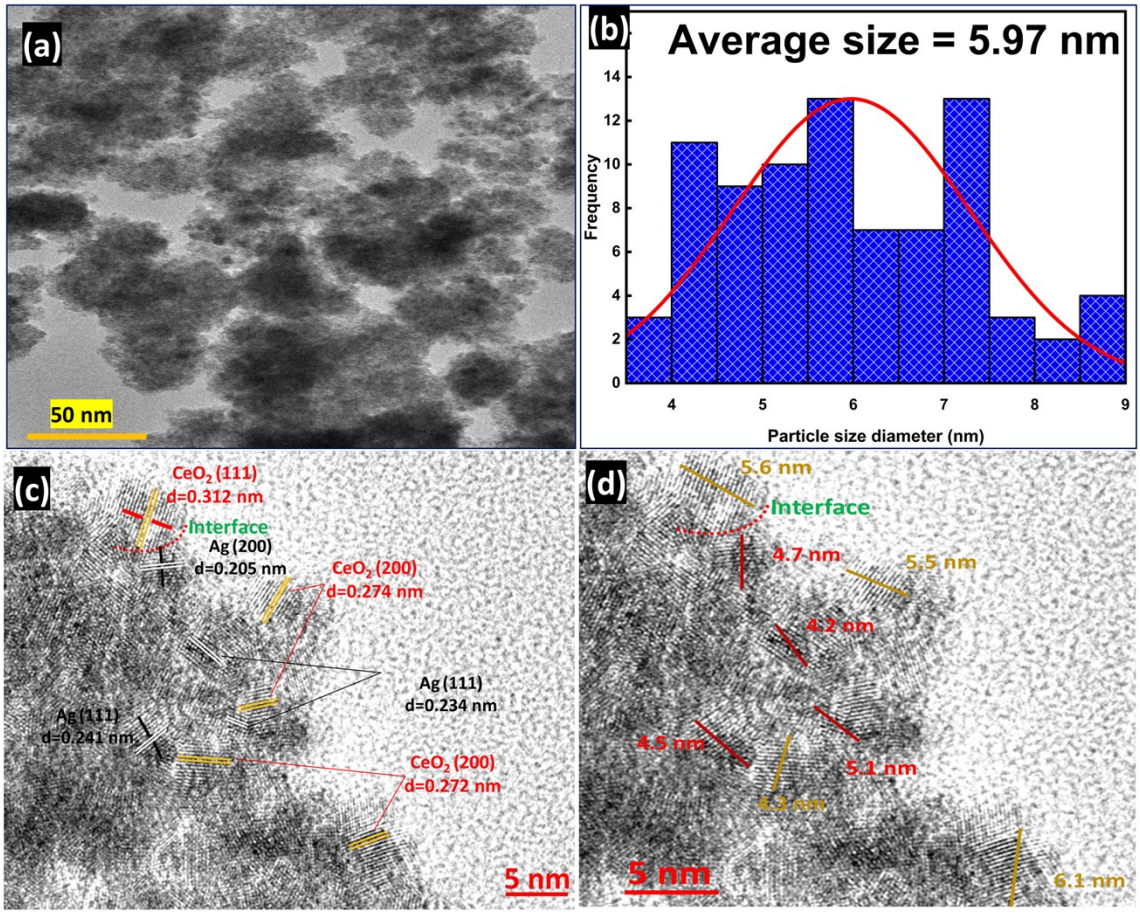

Fig. S7 (a) Low resolution TEM image and (b) calculated average size for Ag/CeO_2, (c) interplanar spaces and (d) average size calculated to individually the Ag and CeO_2.

Fig. **S8a** presents the Nyquist plot obtained from the electrochemical impedance spectroscopy (EIS) of NiF/CeO_2 and NiF/Ag/CeO_2 electrodes, measured in 1 M KOH with a 10-mV amplitude over a frequency range of 10^5–100 Hz. The solution resistance (R_{ct}) was found to be 6.6 Ω. The charge transfer resistance (R_{ct}) for the NiF/CeO_2 and NiF/Ag-CeO_2 electrodes was calculated to be 5.8 Ω and 3.4 Ω, respectively. The lower charge transfer resistance of the NiF/Ag/CeO_2 electrode compared to the NiF/CeO_2 electrode indicates enhanced charge transfer efficiency in the NiF/Ag/CeO_2 system. **Fig. S8b** shows the current vs time curve for the NiF/Ag/CeO_2 electrode under illumination, demonstrating that the electrode-maintained stability throughout the experiment.

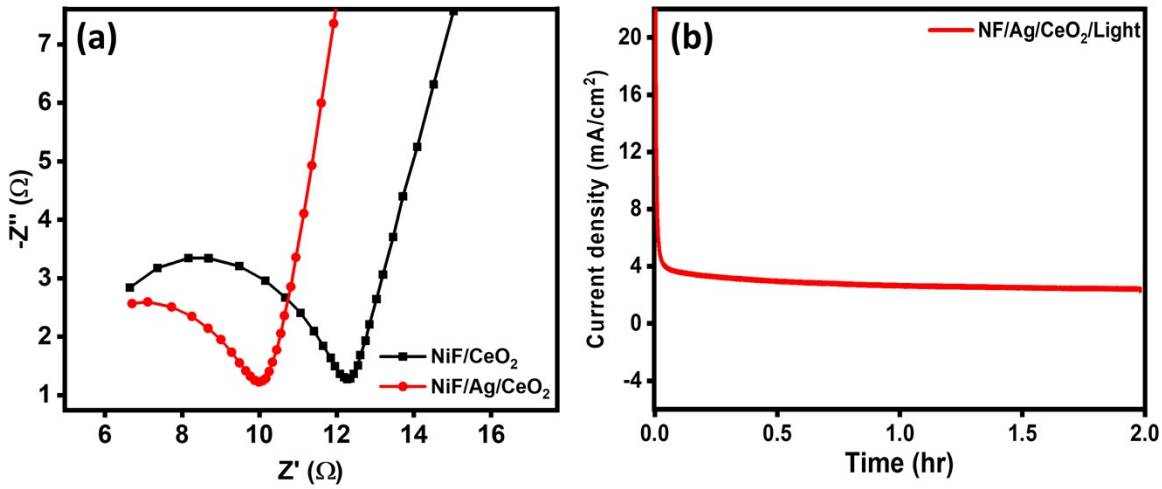

Fig. S8 (a) Nyquist Plot (EIS) for NiF/CeO_2 and NiF/Ag/CeO_2 electrodes, measured in 1 M KOH with a 10-mV amplitude over a frequency range of 10^5–100 Hz (b) Chronoamperometric curve at a constant potential of 1.6 V (vs RHE) for the NiF/Ag/CeO_2 electrode under illumination.

1. Jiang, D., Wang, W., Gao, E., Sun, S., & Zhang, L. (2014). Highly selective defect-mediated photochemical CO_2 conversion over fluorite ceria under ambient conditions. *Chemical communications*, *50*(16), 2005-2007. https://doi.org/10.1039/C3CC47806H

2. Sungu Akdogan, C. Z., Gokcal, B., Polat, M., Hamaloglu, K. O., Kip, C., & Tuncel, A. (2022). Porous, Oxygen Vacancy Enhanced CeO_{2-x} Microspheres with Efficient Enzyme-Mimetic and Photothermal Properties. *ACS Sustainable Chemistry & Engineering*, *10*(29), 9492-9505. https://doi.org/10.1021/acssuschemeng.2c01981

3. Liyanage, A. D., Perera, S. D., Tan, K., Chabal, Y., & Balkus Jr, K. J. (2014). Synthesis, characterization, and photocatalytic activity of Y-doped CeO_2 nanorods. *Acs Catalysis*, *4*(2), 577-584. https://doi.org/10.1021/cs400889y